J Appl Electrochem (2009) 39:39–44
DOI 10.1007/s10800-008-9637-9

ORIGINAL PAPER

Synthesis and characterization of nano-sized calcium zincate powder and its application to Ni–Zn batteries

Chen-Chen Yang · Wen-Chen Chien · Po-Wei Chen · Cheng-Yeou Wu

Received: 20 January 2008 / Accepted: 7 July 2008 / Published online: 15 August 2008

Abstract Nano-sized calcium zincate powders used as active materials for a secondary Zn electrode were prepared by a chemical co-precipitation method. The properties were studied by thermal gravimetric analysis (TGA), micro-Raman spectroscopy and nitrogen adsorption–desorption experiments. The secondary Zn electrodes using chemical co-precipitation calcium zincate powders (CP-ZnCa) and ball-milled calcium zincate powders (BM-ZnCa), were examined and compared. The electrochemical performance of the secondary Zn electrodes was systematically investigated by cyclic voltammetry and galvanostatic charge/discharge measurements. It was demonstrated that the electrochemical properties of the secondary Zn-pasted electrode using CP-ZnCa powders were greatly improved, as compared with conventional secondary ZnO electrodes. The results indicated that secondary Ni-Zn batteries using CP-ZnCa powders exhibited a better charge/discharge property and a longer life-cycle performance, compared with those based on ball-milled ZnO + $Ca(OH)_2$ (BM-ZnCa) powders.

Keywords Zn pasted electrode · Calcium zincate powders · Chemical process · Ni–Zn · Micro-Raman

1 Introduction

The secondary Zn electrode in Zn-air batteries has the following advantages: high specific energy density, low cost and environmental friendliness [1–8]. However, the use and development of the secondary Zn electrode are still limited because of the dendritic growth, shape change, and high solubility of the zinc discharge product in concentrated alkaline KOH solution. These problems are responsible for the short life-cycle of a Zn-paste electrode and the poor electrochemical battery performance. In order to eliminate Zn dendrite formation, many solutions have been sought, including the use of additives either in the electrode [9–11] or in the electrolyte [12–15]. Zhang et al. [16] studied the effect of three organic corrosion inhibitors on the Zn electrode for Zn–MnO_2 batteries by polarization analysis and the electrochemical impedance method. Wang et al. [17] examined the effectiveness of the bismuth ion (Bi^{3+}) and the tetra-butyl ammonium bromide (TBAB) on the Zn electrode to inhibit the dendritic growth in alkaline zincate solution. They found that both Bi^{3+} and TBAB showed a synergistic effect on dendrite inhibition at the Zn electrode.

Recently, some authors [18–21] have reported the performance of secondary Zn-pasted electrodes based on calcium zincate powder as the active material. Calcium zincate ($CaZn_2(OH)_2 \cdot H_2O$) was obtained by mechanical ball milling of ZnO and $Ca(OH)_2$ (so-called BM-ZnCa) in a water medium. Since calcium zincates have a lower solubility in a concentrated KOH solution and a better charge/discharge reversibility, they can solve the problems of shape change and dendrite formation to enhance the life-cycle of the Zn electrode. Yu et al. [20] studied the electrochemical properties of calcium zincates in a secondary Ni-Zn cell by a powder microelectrode, which showed good prospects for practical application. Zhang et al. [21] also investigated the influence of metallic bismuth powder as an additive and chemically co-precipitated calcium zincate as an active material for the secondary Zn-pasted electrode. Specifically, it was found that $Ca(OH)_2$ compounds [20, 21] had a

C.-C. Yang (✉) · W.-C. Chien · P.-W. Chen
Department of Chemical Engineering, Mingchi University of Technology, Taipei Hsien 243, Taiwan, ROC
e-mail: ccyang@mail.mcut.edu.tw

C.-Y. Wu
Taiwan Power Research Institute, Taiwan Power Company, Taipei, Taiwan, ROC

significant impact on the performance of secondary Zn electrodes. The addition of $Ca(OH)_2$ to the pasted Zn electrode can significantly reduce the shape change and dendritic deposit formation. For comparison, the electrochemical performance of Zn-pasted electrodes prepared by ball-milled calcium zincate powders (i.e., BM-ZnCa powders) and chemically-precipitated calcium zincate powders (i.e., CP-ZnCa powders) were systematically investigated by galvanostatic charge/discharge measurements, respectively.

In this work, the electrochemical properties of the Zn electrodes using nanosized calcium zincate powders are studied and discussed. A Ni–Zn battery with a Zn-pasted electrode using CP-ZnCa powders was assembled and evaluated.

2 Experimental

2.1 Preparation of calcium-zincate active materials

The CP-ZnCa active materials were prepared by a chemical co-precipitation method, which has been described elsewhere [21, 22]. The CP-ZnCa active materials were synthesized at 60 °C by adding a mixed solution of 35 mL 1 M $Zn(NO_3)_2$ + 15 mL 1 M $Ca(NO_3)_2$ in the required mole ratio slowly to a 100 mL mixed solution of 1.5 M NaOH + 4.5 M NH_4OH. The mixed solution of $Zn(NO_3)_2$ and $Ca(NO_3)_2$ was added slowly to the alkali solution were added (i.e., drop by drop) under ultrasonication. The mole ratio of the Zn:Ca in the CP-ZnCa powders was set at 2.5:1. The resulting mixed solution was continuously stirred at 1,500 rpm for 8 h until a white precipitate was obtained. The white precipitate suspension was further aged at 60 °C for 12 h under continuous stirring. The CP-ZnCa precipitates were then washed in distilled water several times and centrifuged until the pH became 7, then dried at 105 °C overnight. The CP-ZnCa powders were collected and packed in a PE bag for further examination and use.

2.2 Characterization of calcium zincate powders

TGA thermal analysis was carried out using a Perkin Elmer Pyris 7 TGA system, by heating from 25 to 600 °C, under N_2 atmosphere at a heating rate of 10 C min^{-1} with a sample of approximately 10 mg. Micro-Raman spectroscopy analyses were carried out by a Renishaw confocal system with a microscope equipped with a 50x objective and a charge-coupled device (CCD) detector. The Raman excitation source was provided with a 633 nm laser beam which had a beam power of 17 mW and was focused on the powder samples with a spot size of about 1 μm in diameter. The Brunauer-Emmett-Teller (BET) surface area, the pore size, and the pore size distribution of the BM-ZnCa and CP-ZnCa powders were examined by a Micromeritics ASAP2010 system. The peak pore diameter, mesopore area and volume was estimated according to the Barret-Joyner-Halenda (BJH) method.

2.3 Preparation of the Zn pasted electrodes

The secondary Zn-pasted electrode was prepared by a coat-and-press method; the preparation method was similar to Yang's procedure [19]. The chemical composition of the secondary Zn-pasted electrode was as follows: 70 wt.% CP-ZnCa mixture powders, 2 wt.% nano-Cu conductive fillers, 8 wt.% micro-sized Zn powders (Aldrich), 2 wt.% PbO (Aldrich), 3 wt.% Bi_2O_3 (Aldrich) and 15 wt.% PTFE (Du pont, 30J) suspension-binder solution. In particular, about 2wt.% nano-Cu conductive fillers (100 nm) were added to the Zn-pasted electrode to enhance cycleability and utilization [22]. Appropriate amounts of CP-ZnCa powders and additives were first weighed, then mixed and put into an agate pot with a 10 mm diameter agate ball. The weight ratio of the raw materials to the mill ball was set at 1:5. The ball-milled pot was tightly sealed and set into a planetary ball miller (FRITSCH 7). The mechanical ball-milling was carried out at a rotation speed of 700 rpm for 2 h at ambient temperature. The well-mixed powders were then collected in a plastic container for further use.

The resulting CP-ZnCa mixture powders + PTFE binders were further ball-milled at a rotation speed of 300 rpm for 2 h. The well-mixed CP-ZnCa paste was filled into a Ni-foam matrix (with an area of 1 × 1 cm^2), then roll-pressed at 25 °C at a pressure of 120 $kg_f\ cm^{-2}$. The Zn-pasted electrode was dried at 110 °C for 2 h, and then sintered at 360 °C for 40 min. The substrate of the positive electrode was prepared from 4 × 4 cm^2 of nickel foam. The $Ni(OH)_2$ active material (75wt.%) was mixed with graphite (10wt.%), CoO powder (10wt.%) and then with a polytetrafluoroethylene (PTFE) (5wt.%) aqueous suspension as a binder. The mixtures were ground and annealed to obtain a paste. The paste was coated into the nickel foam substrate using a spatula, dried at 110 °C for 1 h, then cold-pressed at 120 $kg_f\ cm^{-2}$. The electrode was soaked in 4 M KOH for 24 h before use. The alkaline Ni-Zn cell was charged for 5 h at C/5, kept for 30 min at open circuit, and then discharged at a C/5 rate to 1.00 V. The charge/discharge cycle tests were performed at room temperature.

2.4 Electrochemical properties measurements

The galvonostatic charge/discharge measurements for the Zn-pasted electrodes (A = 1 cm^2) using CP-ZnCa powders at different pH values were carried out on a three-electrode system. A large area (10 × 10 cm^2) Pt sheet was used as a counter electrode and an Hg/HgO electrode was used as reference. The cyclic voltammetry analyses of the Zn pasted electrodes (A = 1 cm^2) employing CP-ZnCa

powders were carried out in a three-electrode system. The electrolyte was a ZnO-saturated 4 M KOH aqueous solution. The galvanostatic charge/discharge was examined on a secondary Ni–Zn battery (A = 16 cm^2) wrapped with two layers of Celgard 5550 PP/PE separators at charge and discharge rates of C/5. The cut-off potential was set at 1.0 V. The galvanostatic charge/discharge measurements were conducted by an Autolab PGSTAT30 electrochemical system with GPES 4.8 package software (Eco Chime, The Netherlands). All the electrochemical measurements were carried out at ambient temperature.

3 Results and discussion

3.1 TGA analyses for calcium zincate powders

Figure 1 shows the thermal gravimetric analysis (TGA) and differential thermal analysis (DTA) thermographs for BM-ZnCa and CP-ZnCa powders, respectively. BM-ZnCa powders exhibited only one weight-loss step, but CP-ZnCa powders exhibited a two-step weight loss. The TGA thermograph for BM-ZnCa powders with the mole ratio of Zn:Ca = 2.5:1 showed a total weight loss of 5.27% at 600 °C, with a peak decomposition temperature of 404 °C; which is due to $Ca(OH)_2$ decomposition ($Ca(OH)_2 \rightarrow CaO + H_2O$) [22]. Meanwhile, the results showed that CP-ZnCa powders obtained at pH 12 showed a two-stage weight loss. For first stage with a weight loss of about 12–13% (from 100 to 200 °C) was due to the decomposition reaction of $Zn(OH)_2 \rightarrow ZnO + H_2O$ at a peak temperature of 177 °C for ZnCa powders.

The second weight loss at a peak temperature of ~393 °C was also ascribed to the decomposition reaction of $Ca(OH)_2 \rightarrow CaO + H_2O$. It was noted from DTA results in Fig. 1 that the intensity of the second stage weight-loss ($T_{dp,2}$ = 393 °C) for CP-ZnCa powders at pH 12 was much lower and broader as compared with that of the BM-ZnCa powders. This weight-loss implies a lesser amount of $Ca(OH)_2$ in the CP-ZnCa powders. Finally, the CP-ZnCa powders were completely decomposed into the mixture of CaO and ZnO at 600 °C. Thereby, it was demonstrated that the thermal properties of the CP-ZnCa powders were different from those of the BM-ZnCa powders; especially, it was shown that the CP-ZnCa powders contain mainly $Zn(OH)_2$ and $Ca(OH)_2$, while the BM-ZnCa powders contained ZnO and $Ca(OH)_2$.

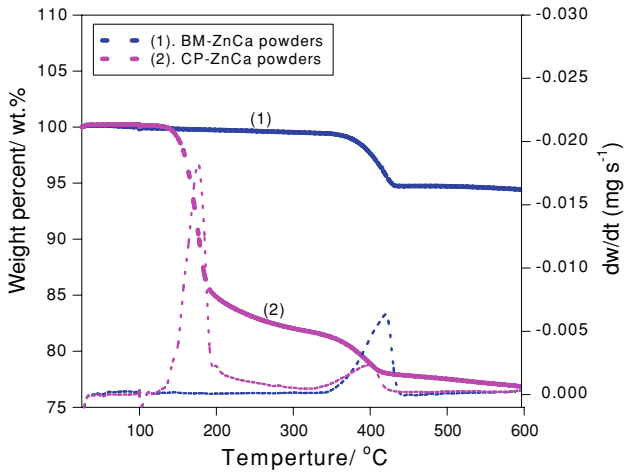

Fig. 1 TGA thermographs for (**a**) ZnO, $Ca(OH)_2$, BM-ZnCa powders; (**b**) CP-ZnCa powders

3.2 The micro-Raman spectroscopy analyses

The micro-Raman analysis was used to examine the chemical composition of raw materials of ZnO, $Ca(OH)_2$ and all of the CP-ZnCa samples. Figure 2 shows the micro-Raman spectra for ZnO, $Ca(OH)_2$, and CP-ZnCa powders at pH 12, respectively. Table 1 lists the major Raman scattering peaks of the ZnO, $Ca(OH)_2$, BM-ZnCa powders and CP-ZnCa powders. There were three major Raman peaks for ZnO, i.e., at 334, 385, and 437 cm^{-1} [22–24]. However, there were four major Raman peaks for $Ca(OH)_2$, namely, at 288, 365, 436, 720 and 1,092 cm^{-1} [22]. In particular, there were five major Raman peaks for CP-ZnCa powders made at pH 12, these Raman peak bands were at 252, 356, 428, 449, 709 and 1,083 cm^{-1}. As we know, the Raman band peaks at 428 cm^{-1} were related to a ZnO compound, but the Raman band peaks at 252, 356, 709 cm^{-1} were related to a $Ca(OH)_2$ compound [22]. All Raman band peak positions for the CP-ZnCa powders were slightly shifted, as compared with the peak positions of

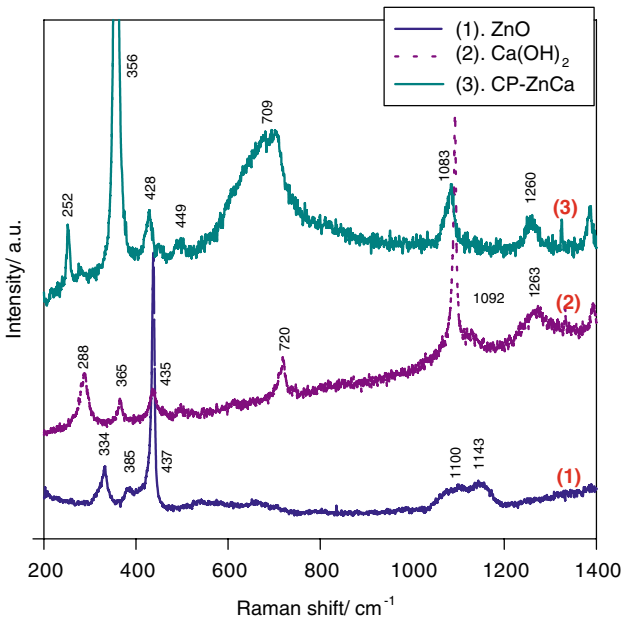

Fig. 2 Raman spectra for ZnO, $Ca(OH)_2$, and CP-ZnCa powders

Table 1 Raman analyses results for ZnO, $Ca(OH)_2$, BM-ZnCa, and CP-ZnCa powders samples

Species	Raman peaks (cm^{-1})
ZnO	334, 385, 437
$Ca(OH)_2$	288, 365, 436, 720, 1,092
BM-ZnCa	321, 425, 561, 648, 1,121
CP-ZnCa	252, 356, 428, 449, 709, 1,083

ZnO and $Ca(OH)_2$. The results indicate that there were some chemical interactions occurring, which may be due to the formation of new chemical bonds between Zn and Ca.

3.3 BET analyses

To obtain detailed information about the pore size, the specific surface area, the mesopore volume and the pore-size distribution, a N_2 adsorption and desorption isotherm were performed on the BM-ZnCa and CP-ZnCa powders. The total surface area and pore volume were determined using the BET equation and the single point method, respectively. Figure 3(a) shows the typical isotherm of N_2 adsorption and desorption (Type IV) for the BM-ZnCa powders and the CP-ZnCa powders. The isotherms exhibited obvious hysteresis loops at high relative pressure (P/P_o), indicating that both ZnCa powders had mainly a mesoporous structure. The surface and volume characteristics of the ZnCa powders calculated according to the isotherm data are summarized in Table 2.

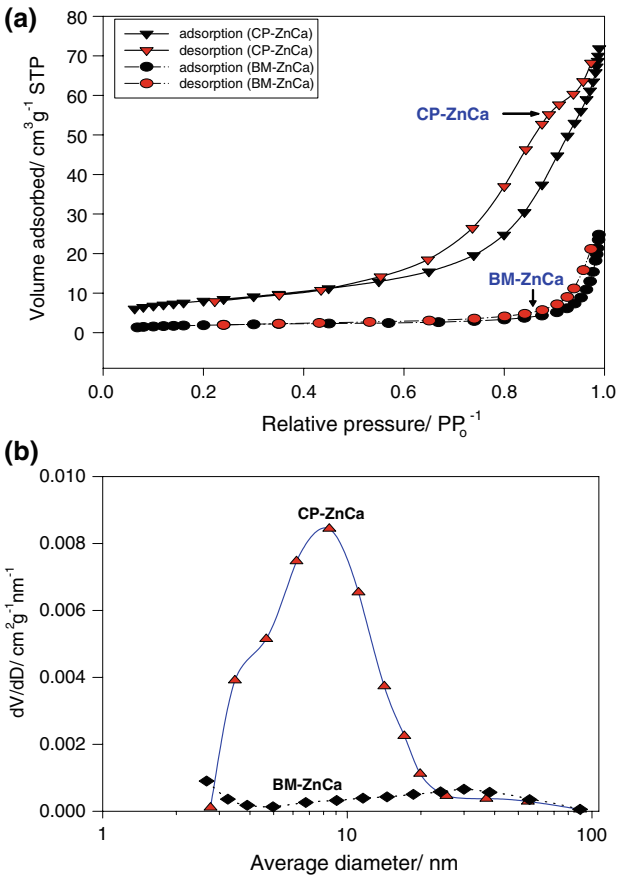

Fig. 3 (**a**) BET isotherm curves for BM-ZnCa and CP-ZnCa powders; (**b**) Pore size distribution curves

In comparison to the BM-ZnCa powders, the CP-ZnCa powders showed a higher BET surface area of 28.66 m^2 g^{-1} and a total pore volume of 0.104 cm^3 g^{-1}; however, the BM-ZnCa powders only showed a BET surface area of 6.72 m^2 g^{-1} and a total pore volume of 0.031 cm^3 g^{-1}. Figure 3(b) demonstrates the pore-size distribution for both the BM-ZnCa and the CP-ZnCa powders. The CP-ZnCa powders possessed a wide pore diameter distribution at 2–100 nm and a peak pore size at 10 nm. In contrast, the BM-ZnCa powders showed much lower pore volume and a narrower pore-size distribution located at a micropore region (<2 nm). It was clear that the porosity and total pore volume of the CP-ZnCa powders prepared by a chemical co-precipitation process were much higher than that of the BM-ZnCa powders by the ball-milled treatment.

3.4 Electrochemical properties

Figure 4 shows the CV curves of the secondary Zn electrode using the CP-ZnCa powders. There were also two cathodic peaks and two anodic peaks on the cyclic voltammograms, the first and second anodic peaks were at −1.32 V ($E_{p,a1}$) and at −1.18 V ($E_{p,a2}$), respectively, for the anodic oxidation of the CP-ZnCa powders. Conversely, there were two cathodic peaks, the first and second cathodic peaks were at −1.37 V ($E_{p,c1}$) and −1.44 V ($E_{p,c2}$), respectively, for the reduction of the CP-ZnCa powder. Table 3 also shows the electrochemical parameters of CV analyses for the Zn-pasted electrodes using CP-ZnCa powders. The CE value of the Zn-pasted electrode using the CP-ZnCa powders (68–70%) was much higher than that of the Zn-pasted electrode using the BM-ZnCa powders (47–53%) during the 200 cycle test. Comparatively, the maximum discharge capability of the CP-ZnCa

Table 2 The results for N_2 adsorption/desorption isotherm for the BM-ZnCa and the CP-ZnCa powders

Types	Parameters		
	BET surface area (m^2 g^{-1})	Total pore volume (m^3 g^{-1})	Pore diameter (nm)
BM-ZnCa powders	6.72	0.031	19.45
CP-ZnCa powders	28.66	0.104	14.73

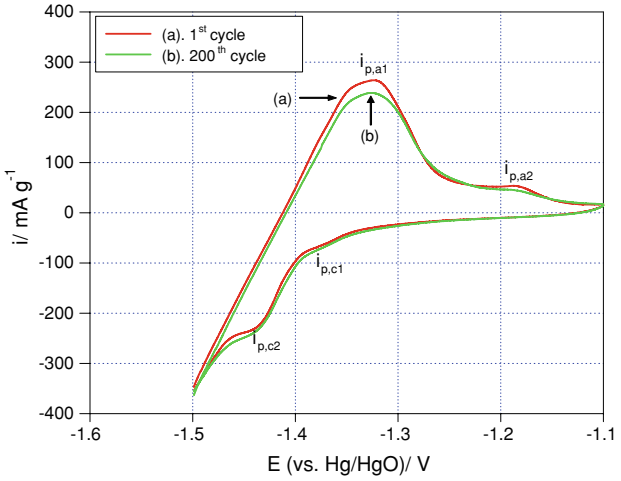

Fig. 4 CV curves of secondary Zn-pasted electrodes with CP-ZnCa powders

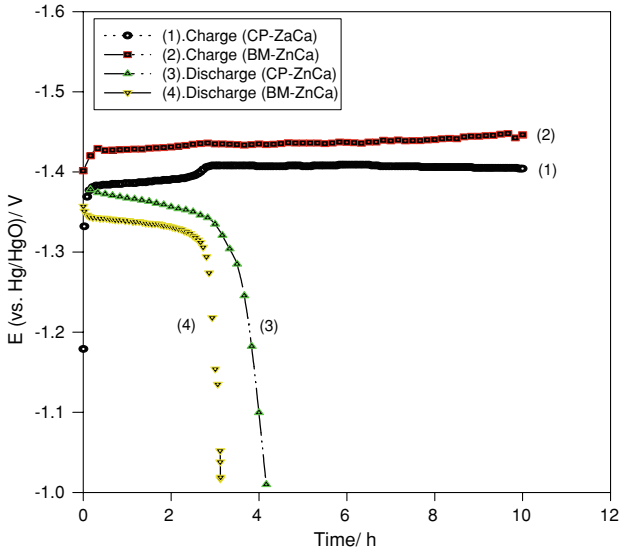

Fig. 5 Charge/discharge curves for secondary Zn-pasted electrodes with BM-ZnCa and the CP-ZnCa powders for comparison

powders ($i_{p,c1}$ = 264 mA g^{-1}) exhibited a much higher value than that of the BM-ZnCa powders ($i_{p,c1}$ = 227 mA g^{-1}). Thus, the chemical precipitation method appears to be an effective process to prepare the active material of the secondary Zn electrode.

Figure 5 shows the charge/discharge curves for the secondary Zn electrodes (A = 1 × 1 cm^2) with the BM- and the CP-ZnCa powders at a charge rate of C/10 and a discharge rate of C/5, respectively. The average charge and discharge potentials of the Zn pasted electrode with BM-ZnCa powders were at −1.436 and −1.327 V (vs. Hg/HgO), respectively. By contrast, the average charge and discharge potentials of the Zn electrode with CP-ZnCa powders were at −1.401 and −1.355 V (vs. Hg/HgO), respectively. The polarization of the secondary electrode with CP-ZnCa powders was much less. Moreover, the CE value for the CP-ZnCa active materials (83.4%) was much higher than that for the BM-ZnCa powders (62.4%). Furthermore, the ΔE values (ΔE is defined as $|E_{ch} - E_{dis}|$, which indicates the reversibility of the electrode) for the CP-ZnCa and the BM-ZnCa active materials were around 0.046 and 0.109 V, respectively. On the whole, it can be concluded that the electrochemical activity of the CP-ZnCa powders is much higher than that of the BM-ZnCa powders.

Figure 6 shows the typical discharge curve of the Ni–Zn battery with the Zn anode using the CP-ZnCa powders

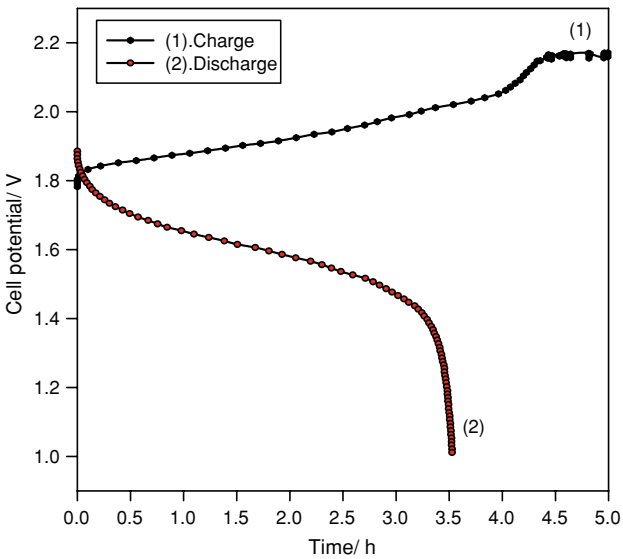

Fig. 6 Typical charge/discharge curve of a Ni–Zn battery at C/5 rate

(prepared at pH 12, theo. capacity ($Q_{theo.}$) = 560 mAh) at C/5 charge/discharge rates. The charge cell potential was stable at between 1.78 and 2.17 V (not shown). The discharge cell potential was also stable and flat at between 1.85 and 1.50 V, which showed an average discharge cell

Table 3 The CV analyses results of the Zn-pasted electrodes using the CP-ZnCa powders

Types	$i_{p,a1}$ (mA g^{-1})	$i_{p,a2}$ (mA g^{-1})	$i_{p,c1}$ (mA g^{-1})	$i_{p,c2}$ (mA g^{-1})	$E_{p.a1}$ (V)	$E_{p.a2}$ (V)	$E_{p.c1}$ (V)	$E_{p.c2}$ (V)	CE (%)
Cyc #1	264	53.7	−70.2	−226	−1.32	−1.18	−1.38	−1.44	70.9
Cyc #200	238	45.3	−72.0	−224	−1.32	−1.18	−1.37	−1.44	68.1

Note: CE(%) = Q_{dis}/Q_{ch} × 100, where the Q_{dis} is a discharge capacity, and the Q_{ch} is a charge capacity

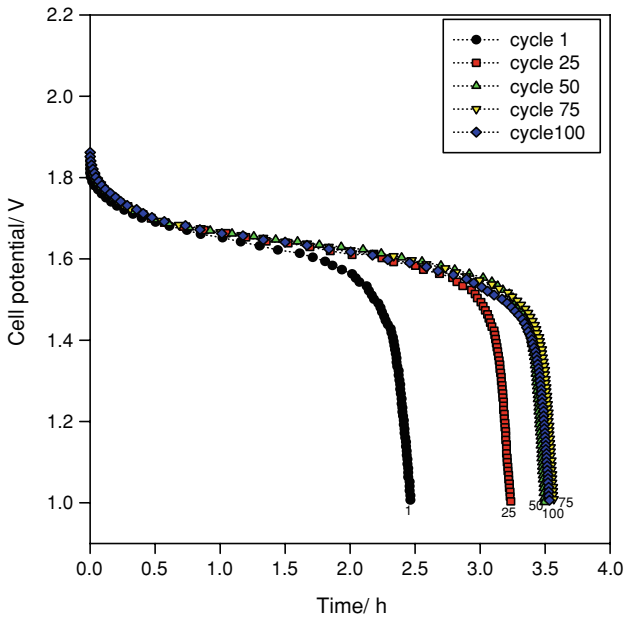

Fig. 7 Charge/discharge curves of Ni–Zn batteries at different cycles

potential of 1.64 V. The cycle life of the Ni–Zn battery was over 100 cycles. The result indicated that the maximum discharge time was 3.53 h. As a matter of fact, the discharge capacity steadily increased after the 50th cycle; the real discharge capacity (depth of discharge = 80%) reached about 71% of theoretical battery capacity ($Q_{theo.}$), as shown in Fig. 7.

4 Conclusions

Calcium zincate powders used as active materials for the secondary Zn-pasted electrodes were prepared by a chemical co-precipitation (CP) method. The characteristic properties of the CP-ZnCa active materials were examined systematically by TGA, micro-Raman spectroscopy and BET analyses. The electrochemical performance of the secondary Zn electrodes using CP-ZnCa powders was examined by cyclic voltammetry and galvanostatic charge/discharge measurements.

It was found that the Zn-paste electrode with the CP-ZnCa powders at a molar ratio of Zn:Ca = 2.5:1 at pH 12 showed good electrochemical performance. The electrochemical properties of CP-ZnCa powders are superior to those of BM-ZnCa powders. The life-cycle of the secondary Ni–Zn batteries was over 100 cycles by galvanostatic charge/discharge measurements at C/5. In conclusion, these CP-ZnCa powders are potential candidates for application in secondary Ni–Zn batteries.

Acknowledgement Financial support from the Taiwan Power Company, Taiwan (Project No: TPC-546-4311-9401B) is gratefully acknowledged.

References

1. Evans JW, Savaskan G (1991) J Appl Electrochem 21:105
2. Savaskan G, Huh T, Evans JW (1992) J Appl Electrochem 22:909
3. Huh T, Savaskan G, Evans JW (1992) J Appl Electrochem 22:916
4. Salas-Morales JC, Evans JW (1994) J Appl Electrochem 24:858
5. Yang H, Cao Y, Ai X, Xiao L (2004) J Power Sources 128:97
6. Zhang C, Wang JM, Zhang L, Cao CN (2001) J Appl Electrochem 31:1049
7. Muller S, Holzer F, Haas O (1998) J Appl Electrochem 28:895
8. Chu MG, McBreen J, Adzic G (1981) J Electrochem Soc 128(11):2281
9. Hang BT (2005) J Power Sources 143:256
10. McLarnon FR, Cairns EJ (1991) J Electrochem Soc 139:645
11. Yang H, Meng X, Yang E, Wang X, Zhou Z (2004) J Electrochem Soc 151(3):A389
12. Ein-Eli Y, Auinat M, Starsvetsky D (2003) J Power Sources 114:330
13. Ein-Eli Y (2004) Electrochem Solid-State Lett 7(1):B5
14. Ein-Eli Y, Auinat M (2003) J Electrochem Soc 150(12):A1606
15. Ein-Eli Y, Auinat M (2003) J Electrochem Soc 150(12):A1614
16. Zhang D, Li L, Cao L, Yang N, Huang C (2001) Corros Sci 43:1627
17. Wang JM, Zhang L, Zhang C, Zhang JQ (2001) J Power Sources 102:139
18. Zhu XM, Yang H-X, Ai X-P, Yu J-X, Cao Y-L (2003) J Appl Electrochem 33:607
19. Yang H, Zhang H, Wang X, Wang J, Meng X, Zhou Z (2004) J Electrochem Soc 151(12):A2126
20. Yu J, Yang H, Ai X, Zhu X (2001) J Power Sources 103:93
21. Zhang C, Wang JM, Zhang L, Cao CN (2001) J Appl Electrochem 31:1049
22. Yang CC, Chien WC, Wang CL, Wu CY (2007) J Power Sources 172:435
23. Music S, Dragcevic D, Popovic S, Ivanda M (2005) Mater Lett 59:2388
24. Chen SJ, Liu YC, Lu YM, Zhang JY, Shen DZ, Fan XW (2006) J Cryst Growth 289:55